

# How to solve the mass-discrepancy problem of SESNe - I. Testing model approximations

Andrea P. Nagy,<sup>1</sup><sup>★</sup>

<sup>1</sup>*Department of Experimental Physics, University of Szeged, Dom ter 9, Szeged, 6720, Hungary*

Accepted XXX. Received YYY; in original form ZZZ

## ABSTRACT

Here, we present a systematic study of 59 stripped-envelope supernovae (SESNe) (including Type IIb, Ib, Ic, and transitional events) to map a possible reason for the so-called mass-discrepancy problem. In this scenario, we assume the tension between the estimated ejected masses from early- and late-time light curves (LC) is due to approximations generally used in analytical models. First, we examine the assumption that the R-band light curve is indeed a good approximation of the bolometric light curve. Next, we test the generally used assumption that rise-time to maximum brightness is equal to the effective diffusion time-scale that can be used to derive the ejecta mass from the early LC. In addition, we analyze the effect of gamma-ray and positron-leakage, which play an important role in forming the shape of the tails of SESNe, and also can be crucial to gaining the ejecta masses from the late-time LC data. Finally, we consider the effect of the different definitions of velocity that are needed for the ejecta mass calculations.

**Key words:** supernovae:general – methods:analytical

## 1 INTRODUCTION

It is generally believed that the death of massive stars ( $M > 8M_{\odot}$ ) form core-collapse supernovae that can be divided into two main groups based on their spectral features. Those explosions that show hydrogen lines in their spectra are classified as Type II, hence those objects that are not labeled as Type Ib/Ic supernovae (e.g., Filippenko 1997; Gal-Yam 2017).

Type Ib and Ic explosions can be separated by the presence or absence of helium in their spectra, however, there are a number of events that can be classified in both types (e.g. SN 1999ex, SN 2002ap, SN 2007gr). That fact indicates that the exact nature of Type Ib/Ic progenitors is not revealed yet. However, the lack of prominent hydrogen and/or helium indicates that during their evolution, the progenitor stars lost most of their outer layers due to interaction with a binary companion, strong stellar wind, or other severe mass-loss processes (e.g., Podsiadlowski et al. 1992; Clocchiatti & Wheeler 1997; Eldridge et al. 2008; Smartt et al. 2009). Moreover, the light curve and spectral properties of Type Ib/Ic supernovae also imply relatively low ejected masses (e.g., Dessart et al. 2011; Taddia et al. 2015; Lyman et al. 2016; Prentice et al. 2016). Due to this latter nature Type Ib/Ic supernovae are also referred to as stripped-envelope SNe (SESNe) (Clocchiatti & Wheeler 1997). Here, it should be noted that Type IIb supernovae, which are identified as a transitional group between hydrogen-rich and hydrogen-poor objects, can also be specified as SESNe, because of their low-mass hydrogen ejecta. Thus, in this paper, we use the terminology of stripped-envelope SNe for both Type Ib/Ic and Type IIb explosions.

Even though the event rate of SESNe is relatively high (about 25%)

among core-collapse supernova (e.g., Shivvers et al. 2017), we still do not understand some basic features of these objects. Theoretical studies (e.g., Clocchiatti & Wheeler 1997; Wheeler et al. 2015) revealed that there is a discrepancy in the derived ejected masses from early- and late-time light curve (LC) fits of stripped-envelope supernovae. Namely, estimations from the post-maximum light variation show systematically higher values than that can be deduced from the light curve peaks by the “Arnett’s rule” (e.g., Khatami & Kasen 2019). To solve this problem, we should take into account two different scenarios. First, it is plausible that the mass-discrepancy occurs due to the limitations and initial boundary conditions of the applied semi-analytic models (e.g., constant Thompson-scattering opacity, spherical symmetry). On the other hand, this mass-discrepancy may have a true physical cause, such as low-mass, low-density ejected, or circumstellar matter (CSM) around the supernova remnant or asymmetries in the explosion (Turatto & Pastorello 2013; Sollerman et al. 2020). Here we concentrate on the first plausible scenario related to the basic assumptions of the generally used semi-analytic light curve models to understand better the mass-discrepancy problem of stripped-envelope SNe from a theoretical point of view.

The paper is organized as follows: in Section 2 we present the data sample. In Section 3 we describe the analytical basis of our model, and explain how we obtain ejected masses from early- and late-time light curves. Section 4 presents our finding related to the difference between the commonly applied model assumptions and our modified initial conditions for both the early- and late-time light curve models. In Section 5 we compare the ejecta masses gained from different approximations. Finally, in Section 6 we summarize our conclusion. In addition, an Appendix is also included where we collect figures showing our best model fits of each supernova.

<sup>★</sup> E-mail: nagyandi@titan.physx.u-szeged.hu

**Table 1.** Basic properties of Type IIb SNe

SN Name	Filter Coverage	Distance (Mpc)	Group
SN1993J	UBVRIJHKL	3.31	1
SN1996cb	BVR	3.8	2
SN2004ex	BVJHYugri	72.8	2
SN2006T	BVJHYugri	32.9	2
SN2006el	BVRr'i'	76.2	2
SN2008aq	UBVJHYugri	26.0	2
SN2008ax	UBVRIJHugri	5.81	2
SN2009mg	UBV	36.4	2
SN2011dh	UBVRIJHK	7.30	2
SN2011fu	UBVRI	82.98	2
SN2011hs	UBVRI	24.5	1
SN2012P	UBVgriz	27.4	1
SN2013df	BVRig'r'i'z'	17.9	2
SN2016gkg	UBVRIgri	26.4	2

**Table 2.** Basic properties of Type Ib SNe

SN Name	Filter Coverage	Distance (Mpc)	Group
SN1983N	UBV	4.60	1
SN1999dn	UBVRIJHK	33.30	2
SN2004gq	UBVRJHugri	24.86	2
SN2007C	UBVRJHugri	23.47	2
SN2007uy	UBVJH	28.98	2
SN2008D	UBVRIJH	29.70	2
SN2009jf	BVJHri	34.44	2
iPTF13bvn	UBVRIgri	19.94	2

## 2 DATA SET

### 2.1 Sample Selection

We begin the data selection by assembling a “master list” of all transients classified as Type Ib/Ic or Type IIb SLSNe in the Open Supernova Catalog (Guillochon et al. 2017), regardless of whether they have been included in a refereed publication or not. This first list of the available SESNe contained 903 events, but most were poorly sampled or missing early- or late-time photometric data. From this, we select the stripped-envelope supernovae with light curves that are well sampled around and after the peak to determine the ejected masses from both early- and late-time light curves. Thus, we identify 59 total SESNe with sufficient data listed in Table 1 - 5. Note that, during the analysis, we divided these supernovae into the following groups: Type Ic, Type Ib, Type Ibc, Type IIb and peculiar (Ic-BL and Ibc-pec). We also separate these supernovae according to their global light curve properties, similar objects, that show increasing or bumpy late-time bolometric light curves (group 1), and the ones that do not (group 2).

### 2.2 Quasi-bolometric Light Curve

To build the quasi-bolometric light curves (LC) of the selected 59 supernovae, we applied the following method. First, we collected the measured magnitudes in all available photometric bands. Then, these data were converted into fluxes using extinctions, distances, and zero points based on (Bessell et al. 1998). The extinction values and distances in each case were taken from NASA/IPAC Extragalactic Database (NED). Photometric data were not equally sampled across all filters, thus, at epochs when the measurements were missing, we

**Table 3.** Basic properties of Type Ibc SNe

SN Name	Filter Coverage	Distance (Mpc)	Group
SN1962L	UBV	5.83	2
SN1998bw	UBVRI	37.9	1
SN1999ex	UBVRI	43.3	2
SN2002ap	UBVRI	6.7	2
SN2005hg	UBVRJHK	81.0	1
SN2006ep	BVJHugri	58.9	2
SN2007Y	UBVugri	19.38	2
SN2007gr	UBVRIJH	9.3	2
SN2009iz	UBVJHri	63.5	2
DES17C1ffz	griz	427.5	2

**Table 4.** Basic properties of Type Ic SNe

SN Name	Filter Coverage	Distance (Mpc)	Group
SN1994I	UBVRI	7.8	2
SN2004aw	UBVRI	74.3	2
SN2004dn	BVRI	50.7	2
SN2004fe	BVRgri	76.13	2
SN2004ff	BVRgri	72.5	2
SN2006lc	BVg'r'i'z'	59.2	2
SN2007cl	Vr'i'	98.7	2
SN2009bb	BVRIJHugri	40.2	1
SN2010bh	BVRiz	274.1	1
SN2010gx	u'g'r'i'z'	1181.3	2
SN2010md	Bgriz	468.8	2
SN2011bm	UBRlugriz	99.0	1
SN2011ke	UBVugriz	697.8	1
SN2011kg	UBJugriz	968.7	1
SN2013dg	griz	1389.0	1
SN2013ge	UBVRiri	15.95	2
SN2014L	UBVRI	14.4	1
SN2014ad	UBVRI	25.3	2
SN2015bn	UBVRIJHKu'g'r'i'z'	544.8	1
PTF15dtg	gri	241.1	1
SN2017ein	UBVRIgr	12.69	2

**Table 5.** Basic properties of peculiar SESNe

SN Name	Filter Coverage	Distance (Mpc)	Group
SN1997ef	V	53.5	2
SN2003dh	UBVRIJH	836.0	2
SN2007bi	BVRI	530.0	1
SN2015U	BVRI	60.3	2
SN2016coi	UBVRIugriz	15.8	1
SN2019dge	ugriz	93.0	2

linearly interpolated the flux using nearby data. The trapezoidal rule was applied while integrating over all wavelength with the assumption that flux reaches zero at 2000 Å. The infrared contribution was taken into account by the exact integration of the Rayleigh-Jeans tail from the wavelength of the last available photometric band to infinity.

## 3 MODEL BASIS

In this study we used our self-developed semi-analytic LC code (Nagy et al. 2014; Nagy & Vinkó 2016), which is based on the radiative diffusion model originally developed by Arnett & Fu (1989).

During the light curve fits, we assumed homologous expansion, spherically symmetric supernova ejecta, constant density profile, and constant opacity. We also suppose that the bolometric luminosity ( $L_{bol}$ ) of the stripped-envelope supernovae is only determined by the energy generated from the radioactive heating of nickel and cobalt. Hence, the spin-down of a low-energy magnetar could be an alternative energy source (e.g., Kasen & Bildsten 2010; Inserra et al. 2013) beside radioactivity (see details in our forthcoming paper).

Because of the supposedly low ejected mass, the effect of gamma-ray and positron leakage was also taken into account as

$$L_{bol} = L_{Ni} (1 - \exp(-T_0^2/t^2)) + M_{Ni} \left[ E_{ki} + E_{Co} (1 - \exp(-T_0^2/t^2)) \right] (1 - \exp(-T_p^2/t^2)), \quad (1)$$

where  $L_{Ni}$  is energy released from radioactive heating (Arnett & Fu 1989; Nagy et al. 2014),  $E_{ki}$  and  $E_{Co}$  are constants (Nadyozhin 1994), and  $T_g$  and  $T_p$  factors are referred to the characteristic time-scale of gamma-ray and positron leakage, respectively.

Using this fitting method, we should be able to obtain the approximate mass of the supernova ejecta, but for most of SESNe, this solution is quite complicated due to their peculiar luminosity gradient at late-times. Hence in this context, we tried not only to simulate the entire bolometric light curve as accurately as possible, but we also adjusted the ejected masses separately from fits to the peak and tail data.

To estimate ejected masses from the early-time LC, we applied the following equation:

$$M_{ej} \approx \frac{\beta c}{2 \kappa} v_{sc} t_d^2, \quad (2)$$

where  $\beta = 13.8$  is an integration constant,  $c$  is the speed of light,  $\kappa$  is the constant opacity,  $v_{sc}$  is the scaling velocity and  $t_d$  is the effective diffusion time-scale. In the literature the accepted definition of  $v_{sc}$  for a constant density ejecta is

$$v_{sc}^2 = \frac{10 E_{kin}}{3 M_{ej}}, \quad (3)$$

where  $E_{kin}$  is the kinetic energy of the supernova explosion. However, the scaling velocity is not related directly to any observable velocities, thus, during the calculations, other definitions were also used (see details in Sect. 4.2).

For the late-time tail, we adopt the following equation to calculate the ejected mass:

$$M_{ej} \approx \sqrt{\frac{T_0^2 E_{kin}}{C \kappa_\gamma}} = \frac{4 \pi T_0^2 v_{sc}^2}{3 \kappa_\gamma}, \quad (4)$$

where  $\kappa_\gamma = 0.028 \text{ cm}^2/\text{g}$  is the gamma-ray opacity (Colgate et al. 1980), and  $C$  is a dimensionless constant dependent on the slope of the density profile. For example  $C \approx 0.07$  for a constant density ejecta.

## 4 TESTING USUAL MODEL ASSUMPTIONS

In order to map the main reasons for the tension between the estimated ejected masses from early- and late-time light curves, we tested separately assumptions generally used for both.

### 4.1 R-band vs. Bolometric LC

According to some preceding papers (e.g., Wheeler et al. 2015), the R-band light curve is a good approximation of the bolometric light

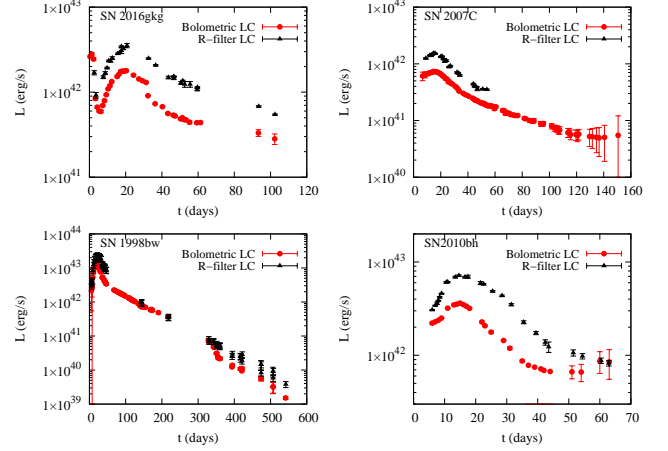


**Figure 1.** Example for the comparison of the R-band (black dots) and bolometric (red dots) LCs of different supernova types.

curve. To test the effect of this assumption, we compare the bolometric light curves of 25 SNe with their R-band luminosity data.

To gain R-band luminosities, we first calculate the absolute magnitudes ( $M$ ) using the distance modulus. Then we take into account the bolometric correction as  $BC \approx -0.3^m$  (Lyman et al. 2014) to determine the bolometric magnitude of the supernova ( $M_{bol} = M + BC$ ). And finally, the following equation was used to calculate the luminosities from R-band data:

$$\log L = -\frac{M_{bol} - M_\odot}{2.5} + \log L_\odot, \quad (5)$$

where  $M_\odot$  and  $L_\odot$  are the bolometric magnitude and the luminosity of the Sun, respectively.

For this analysis, we compare the maximal luminosities and the widths of the peak for both the R-band ( $\Delta t_R$ ) and bolometric ( $\Delta t_{bol}$ ) light curves. As can be seen in Table 6, we get a slightly different result for the different supernova types. For Type IIb and Ibc supernovae, the rise times, the width of the peaks, and the slope of the late-time LCs are not correlated (see e.g. in Fig. 1.) in most cases. However, for Type Ib and Ic, only the near maximum light curves may cover each other by calibrating the luminosities. Thus, scaling the R-band light curve is not usually a plausible solution.

For quantitative analysis, we fit both the R-band and bolometric data and compare the ejected masses, which indicates a significant (up to 30%) difference in the derived results. However, the ratio between  $M_{ej}$  gained from early- and late-time fits show no notable differences. Thus, this approximation is not fully adequate to estimate the physical properties of the individual supernovae, but it does not make a considerable effect on solving the mass-discrepancy problem.

### 4.2 Velocity Assumptions

As it was mentioned above, to calculate ejected masses from both early- and late-time light curves, we need to know the value of the scaling velocity that is not related directly to any observable properties. Thus, during the calculations an approximation for  $v_{sc}$  should be taken into account.

One possibility is that the scaling velocities are derived from LC modeling. However, these values are always somewhat uncertain because of the parameter correlations (Nagy et al. 2014) that may lead to a significant systematic error in the calculated ejected masses. Here, we create generally acceptable fits for the entire supernova light curves, and its  $v_{sc}$  was used as a reference.

**Table 6.** Comparing R-band and bolometric light curve

SN Name	$\Delta t_R$ (days)	$\Delta t_{bol}$ (days)	$L_R/L_{bol}$
SN1996cb	27.7	23.3	1.83
SN2006el	38.4	25.9	1.91
SN2011hs	19.3	19.3	2.81
SN2016gkg	35.5	28.6	1.89
SN1998bw	23.1	18.9	1.67
SN1999ex	28.4	24.3	2.15
SN2002ap	23.2	22.8	2.27
SN2005hg	24.5	24.5	2.07
SN2007gr	20.9	20.9	5.58
SN1999dn	21.0	21.0	2.02
SN2007C	17.2	17.2	2.04
SN2008D	26.1	26.1	2.39
SN1994I	17.1	17.1	2.32
SN2004aw	27.3	27.3	2.33
SN2004dn	15.7	15.7	2.57
SN2004fe	14.9	12.9	2.39
SN2004ff	9.8	9.8	2.55
SN2009bb	20.7	20.7	1.77
SN2010bh	19.7	13.9	2.07
SN2011bm	50.7	48.5	1.74
SN2013ge	30.3	30.3	2.34
SN2014L	22.4	22.4	2.53
SN2014ad	14.8	14.8	2.79
SN2016coi	20.1	20.1	2.95
SN2017ein	21.4	21.4	2.26

Another plausible solution could be that the photospheric velocity ( $v_{ph}$ ) is approximately equal to the scaling velocity. However, in practice,  $v_{ph}$  could be diverse for different chemical elements, and it can also be affected by the density distribution as well as the opacity. Hence, this assumption does not describe well the fixed scaling velocity.

A further assumption could be that we use an average expansion velocity ( $\bar{v}$ ), depending on the supernova type, as the scaling velocity. For example for Type Ib/Iib, Type Ibc and Type Ic 9000 km/s, 9500 km/s and 10000 km/s, respectively. This approximation could define the velocities of such supernovae that do not have spectroscopic data.

Nevertheless, these definitions of the velocity show significantly different values for the individual supernovae (see in Table 7). Hence the ejected mass is sensitive to the choice of the velocity, we calculate  $M_{ej}$  with both approximations, and compare all of the derived results for both early- and late-time models.

### 4.3 Gamma-ray vs. Positron-leakage

It is a generally used approach in the literature that we neglect the partial leakage of the positrons, which is a good approximation as far as the mass of the ejecta is high enough (e.g., for Type IIP) to forbid the fast leakage of the gamma-rays. But for SNe with lower ejected masses, like stripped-envelope ones, the contribution of the positrons will be significant.

The motive, why this approximation seems reasonable is that the time-scale of the positron leakage is much longer than the average length of the SESNe light curves. Thus, positrons should not play an important role in forming the shape of the late-time light curves because of their enormous (around 400 - 2000 days)  $T_p$  values. However, from a modeling point of view using both gamma-ray and

**Table 7.** Velocity values of SESNe

SN Name	$\bar{v}$ (km/s)	$v_{ph}$ (km/s)	$v_{sc}$ (km/s)
SN1993J	9000	7500	14100
SN1996cb	9000	9000	10900
SN2004ex	9000	-	14100
SN2006T	9000	7500	17500
SN2006el	9000	11000	12900
SN2008aq	9000	-	13700
SN2008ax	9000	8000	25100
SN2009mg	9000	10000	16000
SN2011dh	9000	6900	21800
SN2011fu	9000	11000	16400
SN2011hs	9000	8000	14100
SN2012P	9000	-	16200
SN2013df	9000	10800	13800
SN2016gkg	9000	-	12000
SN1983N	9000	7800	10400
SN1999dn	9000	10000	11600
SN2004gq	9000	13000	7000
SN2007C	9000	11000	14500
SN2007uy	9000	14000	4700
SN2008D	9000	10000	8600
SN2009jf	9000	10000	5900
iPTF13bvn	9000	8700	7500
SN1962L	9500	6200	10200
SN1998bw	9500	14000	8200
SN1999ex	9500	-	12500
SN2002ap	9500	15000	9700
SN2005hg	9500	9000	9500
SN2006ep	9500	9500	8900
SN2007Y	9500	9000	12400
SN2007gr	9500	6400	6000
SN2009iz	9500	-	7000
DES17C1ffz	9500	-	11500
SN1994I	10000	11500	8100
SN2004aw	10000	16000	8500
SN2004dn	10000	12500	12000
SN2004fe	10000	11000	14300
SN2004ff	10000	11000	8500
SN2006lc	10000	-	12500
SN2007cl	10000	-	10000
SN2009bb	10000	18000	10900
SN2010bh	10000	30000	11600
SN2010gx	10000	22900	8000
SN2010md	10000	-	7800
SN2011bm	10000	7500	9000
SN2011ke	10000	-	7500
SN2011kg	10000	-	8000
SN2013dg	10000	18000	8500
SN2013ge	10000	10000	12000
SN2014L	10000	7600	14700
SN2014ad	10000	-	13700
SN2015bn	10000	6500	9800
PTF15dtg	10000	6000	10800
SN2017ein	10000	9300	14900
SN1997ef	10000	9500	9200
SN2003dh	10000	-	11100
SN2007bi	10000	-	5000
SN2015U	9000	-	18600
SN2016coi	10000	14000	6500
SN2019dge	9000	8000	25400

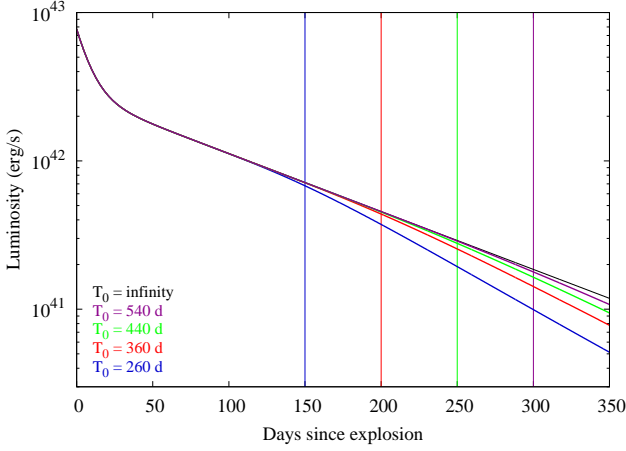


**Figure 2.** Examples for LC tail deflections due to different  $T_0$  values. Vertical lines show the time-scale, where a particular colored line starts to differ from the Ni-Co tail. The  $T_0 = \infty$  (black curve) represents the lack of the gamma-and positron-leakage. Thus, this curve is equal to the nickel-cobalt tail.

positron leakage does not just add an extra energy source at very late times, but also reduces  $T_0$ , which not just causes lower derived ejected masses from the tail, but also reduces the time-scale, when the late-time light curve diverges from the nickel-cobalt tail (Fig. 2.).

To test this theory, we fit the late-time light curve of all SESNe with a  $\chi^2$  method using only gamma-ray, as well as both gamma-ray and positron leakage, and then calculate the ejected masses from them. For simplicity we distinguish the most important parameters ( $T_0$ ,  $M_{Ni}$  and  $M_{ej}$ ) for the case, where only gamma-ray leakage is employed (and the effect of positrons are just ignored) as  $T_\gamma$ ,  $M_{Ni,\gamma}$  and  $M_\gamma$ , while we use  $T_+$ ,  $M_{Ni,+}$  and  $M_+$  for the other scenario.

As can be seen in the Appendix (Fig. A1 - A5), both scenario are capable of reproducing the same late-time LCs. However, using both processes causes significantly lower nickel masses (see in Table 8) that is more reasonable for SESNe (e.g., Sawada & Maeda 2019). It is also noticeable that some fits needed an extremely high nickel mass to generate the LC which may suggest an extra energy input besides radioactive decay. The detailed analysis of this phenomenon is beyond the scope of this paper (see details in our forthcoming paper).

The results also show that the addition of the positron-leakage reduces the  $T_0$  value in most cases, except for two objects (SN 2013df, SN 2019dge). For these supernovae, inconsistency may occur due to the lack of observational data at later times. Moreover, there are some supernovae that despite their low ejecta masses, follow the Ni-Co tail. Thus, their late-time fits result in the upper limit (600 days) for  $T_0$ , which indicates that basically all gamma-rays are trapped inside the ejecta.

#### 4.4 Rise-time vs. Effective Diffusion Time-scale

As it was mentioned in Section 3., we fit the entire bolometric light curve of each supernova. As a fitting parameter, we derive the ejecta masses ( $M_{ej}$ ) from which we were able to calculate the effective diffusion time-scales ( $t_d$ ). So, hereafter we use these  $t_d$  values as a reference to examine the contradiction between the effective diffusion time-scale and the rise time.

From a modeling point of view, we may neglect light curve fitting to determine the ejecta mass if we can somehow estimate the effective diffusion time-scale. An easy way to do so is if  $t_d$  is as-

**Table 8.**  $T_0$  values from different gamma-ray leakage assumptions

SN Name	$T_\gamma$ (d)	$T_+$ (d)	$M_{Ni,\gamma}$ ( $M_\odot$ )	$M_{Ni,+}$ ( $M_\odot$ )
SN1993J	114.7	113.6	0.085	0.042
SN1996cb	109.9	107.1	0.0034	0.0017
SN2004ex	96.0	91.2	0.063	0.032
SN2006T	101.6	99.1	0.06	0.03
SN2006el	117.5	117.4	0.053	0.026
SN2008aq	96.0	93.8	0.03	0.015
SN2008ax	96.3	92.7	0.089	0.045
SN2009mg	121.6	115.8	0.026	0.013
SN2011dh	112.5	109.2	0.048	0.024
SN2011fu	191.0	190.6	0.2	0.098
SN2011hs	600.0	600.0	0.008	0.008
SN2012P	138.6	120.0	0.027	0.014
SN2013df	49.9	66.7	0.05	0.02
SN2016gkg	203.3	202.9	0.055	0.027
SN1983N	149.1	131.1	0.29	0.16
SN1999dn	250.0	250.0	0.024	0.012
SN2004gq	127.2	114.0	0.029	0.015
SN2007C	113.8	108.5	0.019	0.0096
SN2007uy	157.9	154.9	0.0133	0.0066
SN2008D	95.9	95.7	0.0158	0.008
SN2009jf	141.0	138.8	0.2	0.099
iPTF13bvn	135.9	135.4	0.017	0.009
SN1962L	219.9	43.7	0.0029	0.0019
SN1998bw	156.6	151.8	0.3	0.15
SN1999ex	49.4	42.0	0.042	0.025
SN2002ap	125.6	125.4	0.043	0.022
SN2005hg	600.0	600.0	0.047	0.047
SN2006ep	133.4	129.4	0.026	0.013
SN2007Y	80.5	66.4	0.026	0.015
SN2007gr	135.9	131.6	0.0102	0.0055
SN2009iz	111.0	110.8	0.114	0.057
DES17C1ffz	112.1	111.4	0.159	0.081
SN1994I	92.8	88.9	0.0095	0.0048
SN2004aw	361.4	350.4	0.058	0.029
SN2004dn	107.3	103.7	0.026	0.013
SN2004fe	45.6	41.0	0.049	0.031
SN2004ff	600.0	600.0	0.0067	0.0067
SN2006lc	125.6	114.2	0.02	0.01
SN2007cl	72.8	70.3	0.057	0.029
SN2009bb	58.2	54.1	0.043	0.023
SN2010bh	600.0	600.0	0.046	0.046
SN2010gx	38.0	28.4	9.9	7.6
SN2010md	183.2	146.7	1.8	1.0
SN2011bm	99.0	89.7	0.57	0.2
SN2011ke	44.2	40.8	6.9	3.6
SN2011kg	600.0	600.0	1.8	1.8
SN2013dg	141.7	85.2	2.9	2.9
SN2013ge	185.1	184.8	0.0108	0.0054
SN2014L	600.0	600.0	0.0061	0.0061
SN2014ad	95.8	93.6	0.054	0.027
SN2015bn	600.0	275.9	14.8	10.8
PTF15dtg	600.0	600.0	0.2	0.2
SN2017ein	600.0	600.0	0.002	0.002
SN1997ef	110.1	107.3	0.082	0.041
SN2003dh	330.0	219.5	0.4	0.2
SN2007bi	337.8	337.1	4.9	1.95
SN2015U	56.9	49.9	0.021	0.012
SN2016coi	157.9	152.8	0.072	0.036
SN2019dge	79.7	80.9	0.0094	0.0049

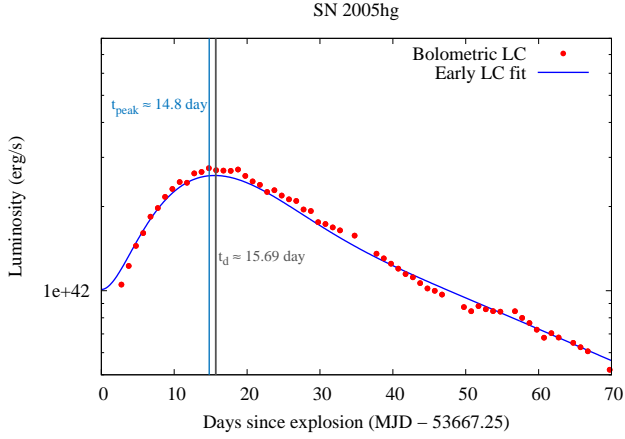


**Figure 3.** Difference between the rise-time and the effective diffusion time-scale for SN 2005hg, where we can estimate the explosion time quite certain because of a non-detection event.

sumed to be equal to the rise time to maximum brightness ( $t_{peak}$ ). However, defining  $t_{peak}$  value is quite uncertain due to the mostly indeterminable explosion time.

Moreover, if we assume that the rise time is roughly equal to  $t_d$  we underestimate the mass. Because, in reality, the rise time is usually much shorter than the effective diffusion time-scale (Fig. 3), which results in lower masses as the expansion velocity is the same. As it can be seen in Table 9 sometimes (mainly for Type IIb SNe) an opposite relation ( $t_{peak} > t_d$ ) occurs. This phenomenon may be explained by an unusually steep peak that is hard to fit properly, or a neglected second component (see details in Nagy & Vinkó (2016)) that prolongs the rise-time.

## 5 COMPARING EJECTA MASSES

Using the results of the early- and late-time light curve calculations allows us to determine the ejecta masses of each scenario. During this process, different velocity estimations were used to compare as many model assumptions as possible. For early LC calculations, we adopt another crucial initial condition, namely, we assume that the average opacity is equal to  $\kappa$  values of the entire light curve fits. However, the  $M_{peak}$  also can be determined by an average Thomson-scattering or a mean hydrodynamic opacities (Nagy 2018) for each supernova type, which definitely changes its value (see details in our forthcoming paper).

As can be seen in Table 10 - 12, using the rise time approximation in most cases underestimates the ejecta masses, while both late-time methods usually overestimate  $M_{ej}$ . But, it is also clear, that applying gamma-ray and positron leakage somewhat reduces the difference between the derived ejected masses and gave more realistic nickel masses.

Overestimation at late-times could be an effect of an unreliable velocity approximation or a misleading LC fit. Both scenarios suggest an interaction with CSM, which may change the slope of the light curve (see group 1 SNe fits) and also reduce the expansion velocity. Another indication of this process can be seen in Fig. 4 which demonstrates a comparison between the derived ejecta masses from scaling velocities. Here, group 1 (objects with irregularities in their LCs) and group 2 SNe do not show any difference, which suggests that all stripped-envelope supernovae, regardless of their visible LCs features, are involved in CSM interaction. This speculation also can

**Table 9.** Rise-time and effective diffusion time-scale of SESNe

SN Name	$t_d$ (d)	$t_{peak}$ (d)
SN1993J	19.61	20.6
SN1996cb	25.73	16.6
SN2004ex	16.89	16.7
SN2006T	18.44	14.0
SN2006el	19.48	12.6
SN2008aq	15.68	10.9
SN2008ax	14.12	16.6
SN2009mg	17.53	14.9
SN2011dh	16.90	19.9
SN2011fu	13.77	16.3
SN2011hs	18.25	13.1
SN2012P	12.15	10.5
SN2013df	21.06	20.1
SN2016gkg	20.65	17.6
SN1983N	15.63	15.4
SN1999dn	19.77	14.0
SN2004gq	15.83	8.3
SN2007C	14.31	9.8
SN2007uy	18.57	15.7
SN2008D	18.92	16.1
SN2009jf	22.92	22.6
iPTF13bvn	15.79	14.1
SN1962L	27.12	17.1
SN1998bw	14.89	14.0
SN1999ex	19.29	15.1
SN2002ap	16.51	10.1
SN2005hg	15.69	14.8
SN2006ep	16.94	12.2
SN2007Y	17.51	15.4
SN2007gr	17.48	11.8
SN2009iz	23.02	17.2
DES17C1ffz	20.43	23.4
SN1994I	13.36	8.1
SN2004aw	17.23	16.0
SN2004dn	14.72	12.8
SN2004fe	9.13	8.8
SN2004ff	19.61	10.6
SN2006lc	21.28	13.6
SN2007cl	21.49	14.4
SN2009bb	13.89	11.2
SN2010bh	15.27	13.0
SN2010gx	48.09	14.7
SN2010md	32.66	32.1
SN2011bm	27.52	27.1
SN2011ke	53.09	24.3
SN2011kg	43.61	23.1
SN2013dg	43.62	5.6
SN2013ge	25.92	16.5
SN2014L	19.90	11.9
SN2014ad	22.18	11.5
SN2015bn	85.37	60.2
PTF15dtg	22.47	21.9
SN2017ein	15.77	14.0
SN1997ef	23.17	16.7
SN2003dh	8.37	2.1
SN2007bi	52.45	22.0
SN2015U	9.49	7.9
SN2016coi	23.99	16.7
SN2019dge	4.22	3.5

**Table 10.** Ejected masses of SESNe calculated from the average expansion velocities ( $\bar{v}$ )

SN Name	$M_{ej} (M_{\odot})$	$M_{peak} (M_{\odot})$	$M_{\gamma} (M_{\odot})$	$M_{+} (M_{\odot})$
SN1993J	2.1	1.48	5.98	5.87
SN1996cb	2.8	1.48	5.49	5.22
SN2004ex	2.6	1.62	4.19	3.78
SN2006T	2.3	1.37	4.69	4.47
SN2006el	3.8	1.11	6.28	6.27
SN2008aq	2.6	0.83	4.19	4.00
SN2008ax	1.77	0.88	4.22	3.91
SN2009mg	1.9	1.55	6.72	6.10
SN2011dh	1.4	0.92	5.76	5.42
SN2011fu	1.0	0.77	16.68	16.52
SN2011hs	2.6	1.20	–	–
SN2012P	1.85	0.71	8.74	6.55
SN2013df	2.37	1.41	1.13	2.02
SN2016gkq	3.6	1.97	18.80	18.72
SN1983N	2.8	2.37	10.11	7.82
SN1999dn	3.5	1.37	28.42	28.42
SN2004gq	3.4	1.19	7.36	5.91
SN2007C	2.3	0.67	5.89	5.35
SN2007uy	6.2	8.63	11.34	10.91
SN2008D	3.4	2.60	4.18	4.17
SN2009jf	4.8	7.12	9.04	8.76
PTF13bvn	4.8	4.62	8.40	8.34
SN1962L	2.9	1.07	27.15	1.07
SN1998bw	4.7	4.84	12.43	11.68
SN1999ex	3.0	1.40	1.24	0.89
SN2002ap	6.8	2.48	7.99	7.97
SN2005hg	3.0	2.70	–	–
SN2006ep	3.8	2.11	9.02	8.48
SN2007Y	2.94	1.75	3.28	2.23
SN2007gr	4.7	3.43	9.36	8.78
SN2009iz	4.1	3.12	6.24	6.22
DES17C1ffz	3.7	4.04	6.37	6.29
SN1994I	2.8	1.27	4.84	4.44
SN2004aw	6.5	6.63	73.33	68.82
SN2004dn	2.0	1.27	6.46	6.04
SN2004fe	2.3	1.50	1.17	0.94
SN2004ff	2.8	0.97	–	–
SN2006lc	2.91	0.96	8.86	7.32
SN2007cl	2.99	1.34	2.98	2.77
SN2009bb	2.7	1.62	1.90	1.64
SN2010bh	2.1	1.31	–	–
SN2010gx	4.75	0.56	0.81	0.45
SN2010md	6.4	8.00	18.84	12.08
SN2011bm	6.6	7.13	5.50	4.52
SN2011ke	5.42	1.53	1.10	0.93
SN2011kg	4.5	1.59	–	–
SN2013dg	3.92	0.08	11.27	4.08
SN2013ge	3.2	1.06	19.24	19.17
SN2014L	2.25	0.55	–	–
SN2014ad	2.6	0.51	5.15	4.92
SN2015bn	13.8	7.03	–	42.74
iPTF15dtg	4.2	3.72	–	–
SN2017ein	2.2	1.17	–	–
SN1997ef	3.8	2.17	6.81	6.46
SN2003dh	1.5	0.09	61.14	27.05
SN2007bi	11.9	4.18	64.07	63.80
SN2015U	1.3	0.44	1.47	1.13
SN2016coi	4.8	3.61	14.00	13.11
SN2019dge	0.7	0.17	2.89	2.98

**Table 11.** Ejected masses of SESNe calculated from the photospheric velocities ( $v_{ph}$ )

SN Name	$M_{ej} (M_{\odot})$	$M_{peak} (M_{\odot})$	$M_{\gamma} (M_{\odot})$	$M_{+} (M_{\odot})$
SN1993J	2.1	1.23	4.16	4.08
SN1996cb	2.8	1.48	5.49	5.22
SN2006T	2.3	1.14	3.26	3.10
SN2006el	3.8	1.36	9.38	9.36
SN2008ax	1.77	0.78	3.33	3.09
SN2009mg	1.9	1.72	8.30	7.53
SN2011dh	1.4	0.71	3.38	3.19
SN2011fu	1.0	0.95	24.78	24.68
SN2011hs	2.6	1.07	–	–
SN2013df	2.37	1.70	1.63	2.91
SN1983N	2.8	2.06	7.59	5.87
SN1999dn	3.5	1.52	35.09	35.09
SN2004gq	3.4	1.72	15.35	12.33
SN2007C	2.3	0.82	8.80	8.00
SN2007uy	6.2	13.43	27.44	26.40
SN2008D	3.4	2.89	5.16	5.14
SN2009jf	4.8	7.91	11.16	10.82
PTF13bvn	4.8	4.46	7.85	7.79
SN1962L	2.9	0.70	10.44	0.41
SN1998bw	4.7	7.13	26.99	25.36
SN2002ap	6.8	3.92	19.93	19.87
SN2005hg	3.0	2.56	–	–
SN2006ep	3.8	2.11	9.02	8.48
SN2007Y	2.94	1.66	2.95	2.01
SN2007gr	4.7	2.31	4.25	3.98
SN1994I	2.8	1.46	6.39	5.87
SN2004aw	6.5	10.60	187.73	176.18
SN2004dn	2.0	1.59	10.10	9.43
SN2004fe	2.3	1.65	1.41	1.14
SN2004ff	2.8	1.07	–	–
SN2009bb	2.7	2.92	6.16	5.32
SN2010bh	2.1	3.94	–	–
SN2010gx	4.75	1.28	4.25	2.37
SN2011bm	6.6	5.35	3.10	2.54
SN2013dg	3.92	0.14	36.53	13.21
SN2013ge	3.2	1.06	19.24	19.17
SN2014L	2.25	0.42	–	–
SN2015bn	13.8	4.57	–	18.06
iPTF15dtg	4.2	2.23	–	–
SN2017ein	2.2	1.09	–	–
SN1997ef	3.8	2.06	6.14	5.83
SN2016coi	4.8	5.05	27.44	25.69
SN2019dge	0.7	0.15	2.28	2.35

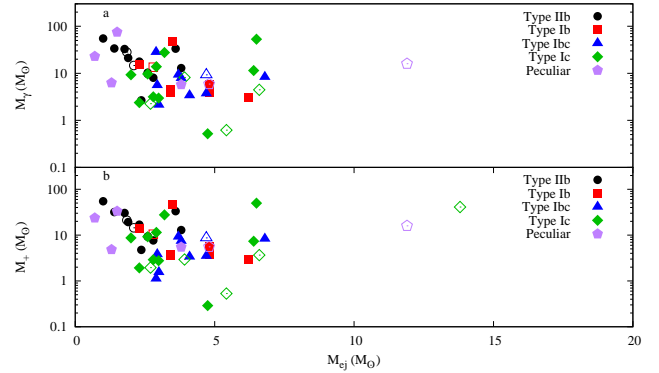
be supported by the single-star progenitor theory, where we assume an extreme mass-loss at the late evolutionary phase.

If we assume a CSM around the exploding star, the generally used homologous expansion may be inaccurate at late times which indicates that we should scale down the velocities for these calculations. However, taking into account the velocity changes could be problematic because we are not able to determine the physical properties of the CSM from our model.

According to basic analytical studies, during the interaction phase, the ratio of late-time and initial velocities ( $\alpha$ ) is about 0.5 - 0.8 depending on the CSM density profile, while in the Sedov phase  $\alpha \sim 0.4$ . The time-scale of these phases could be really different due to the intensity of the CSM interaction. To test our results we systematically calculated this parameter using the assumption that

**Table 12.** Ejected masses of SESNe calculated from the scaling velocities ( $v_{sc}$ )

SN Name	$M_{ej}$ ( $M_{\odot}$ )	$M_{peak}$ ( $M_{\odot}$ )	$M_{\gamma}$ ( $M_{\odot}$ )	$M_{+}$ ( $M_{\odot}$ )
SN1993J	2.1	2.32	14.69	14.41
SN1996cb	2.8	1.80	8.06	7.65
SN2004ex	2.6	2.54	10.29	9.28
SN2006T	2.3	2.66	17.75	16.89
SN2006el	3.8	1.59	12.90	12.88
SN2008aq	2.6	1.26	9.71	9.27
SN2008ax	1.77	2.44	32.80	30.40
SN2009mg	1.9	2.76	21.25	19.27
SN2011dh	1.4	2.23	33.77	31.82
SN2011fu	1.0	1.41	55.09	54.86
SN2011hs	2.6	1.88	–	–
SN2012P	1.85	1.27	28.31	21.22
SN2013df	2.37	2.17	2.66	4.76
SN2016gkg	3.6	2.63	33.42	33.29
SN1983N	2.8	2.74	13.50	10.44
SN1999dn	3.5	1.76	47.22	47.22
SN2004gq	3.4	0.93	4.45	3.58
SN2007C	2.3	1.08	15.29	13.90
SN2007uy	6.2	4.51	3.09	2.98
SN2008D	3.4	2.48	3.82	3.80
SN2009jf	4.8	4.67	3.89	3.77
PTF13bvn	4.8	3.85	5.83	5.79
SN1962L	2.9	1.15	28.25	1.12
SN1998bw	4.7	4.18	9.26	8.70
SN1999ex	3.0	1.84	2.14	1.55
SN2002ap	6.8	2.54	8.33	8.31
SN2005hg	3.0	2.70	–	–
SN2006ep	3.8	1.98	7.91	7.45
SN2007Y	2.94	2.28	5.59	3.81
SN2007gr	4.7	2.17	3.73	3.50
SN2009iz	4.1	2.30	3.39	3.38
DES17C1ffz	3.7	4.89	9.33	9.21
SN1994I	2.8	1.03	3.17	2.91
SN2004aw	6.5	5.63	52.98	49.72
SN2004dn	2.0	1.53	9.31	8.69
SN2004fe	2.3	2.15	2.39	1.93
SN2004ff	2.8	0.82	–	–
SN2006lc	2.91	1.20	13.84	11.44
SN2007cl	2.99	1.34	2.98	2.77
SN2009bb	2.7	1.77	2.26	1.95
SN2010bh	2.1	1.52	–	–
SN2010gx	4.75	0.45	0.52	0.29
SN2010md	6.4	6.24	11.46	7.35
SN2011bm	6.6	6.41	4.46	3.66
SN2011ke	5.42	1.15	0.62	0.53
SN2011kg	4.5	1.27	–	–
SN2013dg	3.92	0.06	8.15	2.94
SN2013ge	3.2	1.27	27.70	27.61
SN2014L	2.25	0.81	–	–
SN2014ad	2.6	0.70	9.67	9.23
SN2015bn	13.8	6.89	–	41.05
iPTF15dtg	4.2	4.02	–	–
SN2017ein	2.2	1.74	–	–
SN1997ef	3.8	1.99	5.75	5.47
SN2003dh	1.5	0.10	75.34	33.33
SN2007bi	11.9	2.09	16.02	15.95
SN2015U	1.3	0.90	6.29	4.84
SN2016coi	4.8	2.35	5.91	5.54
SN2019dge	0.7	4.83	23.01	23.71

**Figure 4.** Comparison of  $M_{ej}$  with  $M_{\gamma}$  (panel a) and  $M_{+}$  (panel b) derived from scaling velocities. The different colors represent the different supernovae types (IIb black, Ib red, Ibc blue, Ic green and peculiar purple), while the empty and filled symbols show group 1 and group 2 SNe within a particular type.

$\alpha \approx v_{mod}/v_{sc} = \sqrt{M_{+}/M_{ej}}$ . We also exclude events with extremely short or uncertain late-time light curves, where  $T_0$  values could be inconsistent. Then, we were able to compare the derived parameters and the theoretical predictions (Table 13). Then, we presume that the average  $\alpha$  for a particular supernovae type could be a reasonable velocity modification constant. For Type IIb, Ib, Ibc, Ic and peculiar SNe this value is 0.39, 0.74, 0.82, 0.67 and 0.87, respectively. Using these we can recalculate the scaling velocities and ejected masses ( $M_{+,mod}$ ) that are now closer to the expected  $M_{ej}$  values in most cases. Thus, with this empirical scaling method, we may reduce the tension between the early and late-time mass estimations.

## 6 CONCLUSIONS

We have presented the results of our systematic study related to stripped-envelope supernova modeling. Our main goal was testing the generally used model approximations in order to make sure that the mass-discrepancy problem is not caused by the initial condition of the applied analytical models.

First, we tested the R-band approximation and our study revealed that in most cases the R-band and the bolometric light curve do not show the same general features (e.g. rise time, decline rate of the tail). Thus, this approximation is not sufficient to estimate the physical properties of individual supernovae. However, the mass ratio of early- and late-time ejected mass calculations do not show significant differences, which indicates that this approximation does not cause the mass-discrepancy problem.

We also took into consideration the rise-time approximation. The main problem with this method is that, except for some recent SESNe, the explosion times are quite uncertain, which causes the underestimation of the ejected mass. However, due to recent all-sky surveys, the determination of the supernova explosion date could be more precise in the near future. Till then, fitting the early light curve and defining the ejected mass from it seems to be a bit more reasonable solution. But, there are some issues in our model to fit the rising phase of the supernova LCs. The solution for this could be an alternative energy source or a two-component model, as our previous study revealed (e.g., Nagy & Vinkó 2016) for Type IIb supernovae.

**Table 13.** Modified scaling velocities and ejected masses of SESNe

SN Name	$\alpha$	$v_{mod}$ (km/s)	$M_{+,mod}$ ( $M_{\odot}$ )	$M_{ej}$ ( $M_{\odot}$ )
SN1993J	0.38	5499	2.19	2.1
SN1996cb	0.60	4251	1.16	2.8
SN2006T	0.37	6825	2.57	2.3
SN2006el	0.54	5031	1.96	3.8
SN2008aq	0.53	5343	1.41	2.6
SN2008ax	0.24	9789	4.62	1.77
SN2011dh	0.21	8502	4.84	1.4
SN2012P	0.30	6318	3.23	1.85
SN2016gkg	0.33	4680	5.06	3.6
SN1983N	0.52	7696	5.72	2.8
SN1999dn	0.27	8584	25.9	3.5
SN2004gq	0.97	5180	1.96	3.4
SN2007C	0.41	10730	7.61	2.3
SN2008D	0.95	6364	2.08	3.4
SN2009jf	1.13	4366	2.06	4.8
PTF13bvn	0.91	5550	3.17	4.8
SN1998bw	0.74	6724	5.85	4.7
SN2002ap	0.90	7954	5.59	6.8
SN2006ep	0.71	7298	5.01	3.8
SN2007Y	0.88	10168	2.56	2.94
SN2007gr	1.16	4920	2.35	4.7
DES17C1ffz	0.63	9430	6.19	3.7
SN2004dn	0.48	8040	3.9	2.0
SN2010md	0.93	5226	3.3	6.4
SN2013dg	1.15	5695	1.32	3.92
SN2013ge	0.34	8040	12.39	3.2
SN2014ad	0.53	9179	4.14	2.6
SN2015bn	0.58	6566	18.4	13.8
SN1997ef	0.83	8004	4.14	3.8
SN2007bi	0.86	4350	12.1	11.9
SN2016coi	0.93	5655	4.19	4.8

The third estimation we tested is related to the ejected mass calculation of late-time supernova light curves. The results show that taking into account both gamma-ray and positron-leakage somewhat reduces the derived ejecta masses due to the lower  $T_0$  values as well as giving more reasonable nickel masses. But, this scenario still overestimates  $M_{ej}$  regardless of the used velocity definition. To moderate this issue we may modify the velocity and/or opacity values or implement a self-consistent  $T_0$  calculation approach in our code.

Overall, our results suggest that the mass-discrepancy problem is not strongly related to the basic approximations, but the mass difference can be reduced with fine-tuning of these estimations, as we show above. Moreover, this also indicates that we should study the physical structure of these objects in more detail and improve our model to consider these characteristics as accurately as possible.

## ACKNOWLEDGEMENTS

Special thanks to John Craig Wheeler for the helpful suggestions and discussions related to the mass-discrepancy problem and this article. This project is supported by NKFIH/OTKA PD- 134434 grant, which is funded by the Hungarian National Development and Innovation Fund.

## DATA AVAILABILITY

The data underlying this article are available in the Open Supernova Catalog, currently at <https://github.com/astrocatalogs>. While, the source code of the program applied for light curve fitting in this paper is available online at <http://titan.physx.u-szeged.hu/nagyandi/LC2>.

## REFERENCES

- Arnett W. D., Fu A., 1989, *ApJ*, 340, 396  
 Bessell M. S., Castelli F., Plez B., 1998, *A&A*, 333, 231  
 Clocchiatti A., Wheeler J. C., 1997, *ApJ*, 491, 375  
 Colgate S., Petschek A., Kriese J., 1980, *ApJL*, 237, 81  
 Dessart L., Hillier D. J., Livne E., Yoon S.-C., Woosley S., Waldman R., Langer N., 2011, *MNRAS*, 414, 2985–3005  
 Eldridge J. J., Izzard R. G., Tout C. A., 2008, *MNRAS*, 384, 1109  
 Filippenko A. V., 1997, *ARA&A*, 35, 309  
 Gal-Yam A., 2017, [https://doi.org/10.1007/978-3-319-21846-5\\_35](https://doi.org/10.1007/978-3-319-21846-5_35), p. 195  
 Guillochon J., Parrent J., Kelley L. Z., Margutti R., 2017, *ApJ*, 835, 64  
 Inserra C., et al., 2013, *ApJ*, 770, 128  
 Kasen D., Bildsten L., 2010, *ApJ*, 717, 245  
 Khatami D. K., Kasen D. N., 2019, *ApJ*, 878, 56  
 Lyman J. D., Bersier D., James P. A., 2014, *MNRAS*, 437, 3848  
 Lyman J. D., Bersier D., James P. A., Mazzali P. A., Eldridge J. J., Fraser M., Pian E., 2016, *MNRAS*, 457, 328–350  
 Nadyozhin D. K., 1994, *ApJSS*, 92, 527  
 Nagy A. P., 2018, *ApJ*, 862, 143  
 Nagy A. P., Vinkó J., 2016, *A&A*, 589, A53  
 Nagy A. P., Ordasi A., Vinkó J., Wheeler J. C., 2014, *A&A*, 571, A77  
 Podsiadlowski P., Joss P. C., Hsu J. J. L., 1992, *ApJ*, 391, 246  
 Prentice S. J., et al., 2016, *MNRAS*, 458, 2973–3002  
 Sawada R., Maeda K., 2019, *ApJ*, 886, 47  
 Shivvers I., et al., 2017, *PASP*, 129, 054201  
 Smartt S. J., Eldridge J. J., Crockett R. M., Mound J. R., 2009, *MNRAS*, 395, 1409  
 Sollerman J., et al., 2020, *A&A*, 643, A79  
 Taddia F., et al., 2015, *A&A*, 547, A60  
 Turatto M., Pastorello A., 2013, *Proceedings of the International Astronomical Union*, 9, 63  
 Wheeler J. C., Johnson V., Clocchiatti A., 2015, *MNRAS*, 450, 1295

## APPENDIX A: LIGHT CURVE FITS OF SESNE

Here, we show the bolometric light curve fits of all examined SESNe. In each figure, the blue line represents the best model for the entire LC due to the fit-by-eye method, while the green and black lines show the calculation results for the two different late-time fitting approaches.

This paper has been typeset from a  $\text{\TeX}/\text{\LaTeX}$  file prepared by the author.

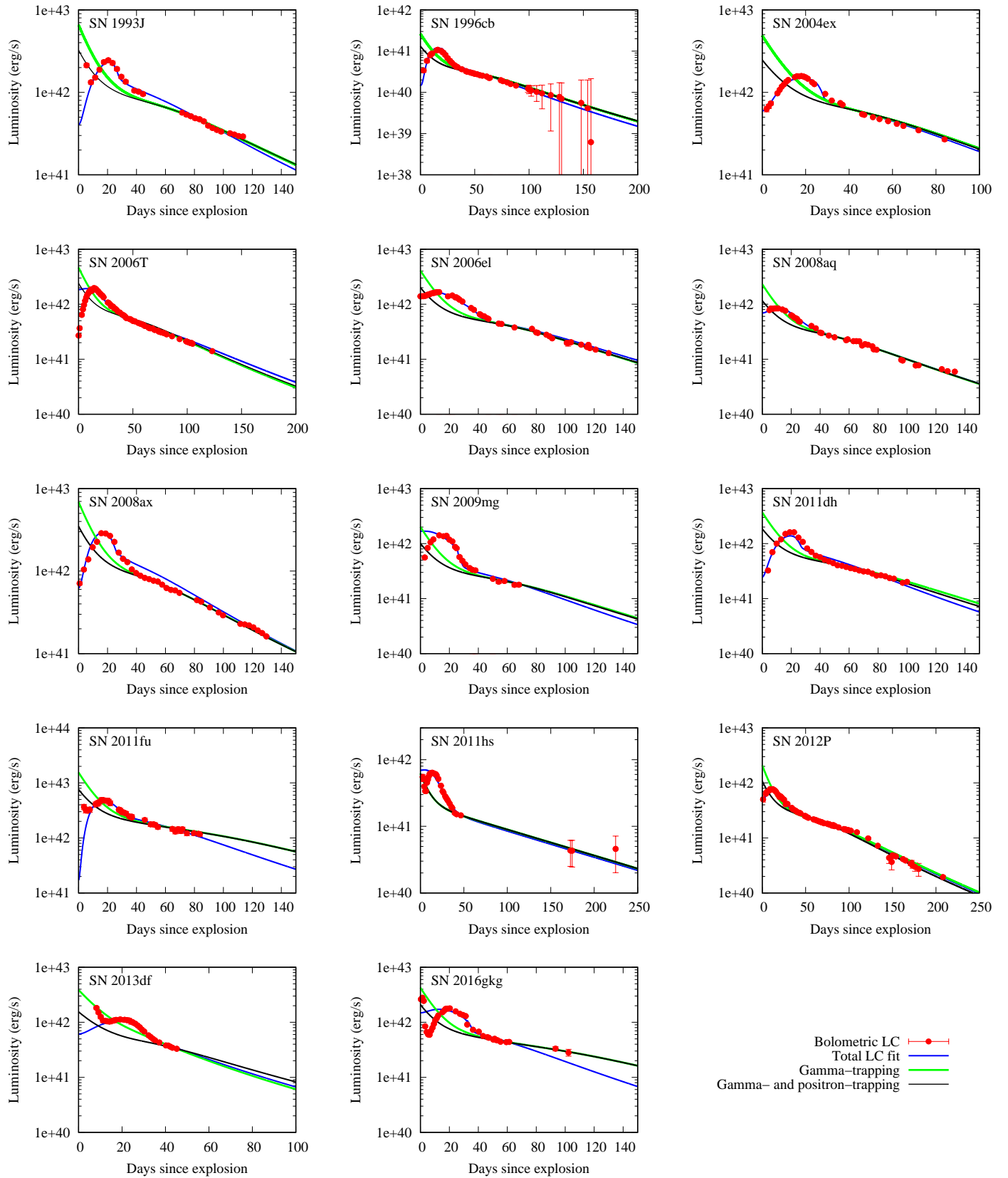


**Figure A1.** Bolometric light curve fits for Type IIb supernovae. The red dots show the observational data with their photometric errors. The blue line represents the best fit for the entire light curve, while the green and black lines show the late-time LC fits for only gamma-leakage and gamma- and positron-leakage, respectively.

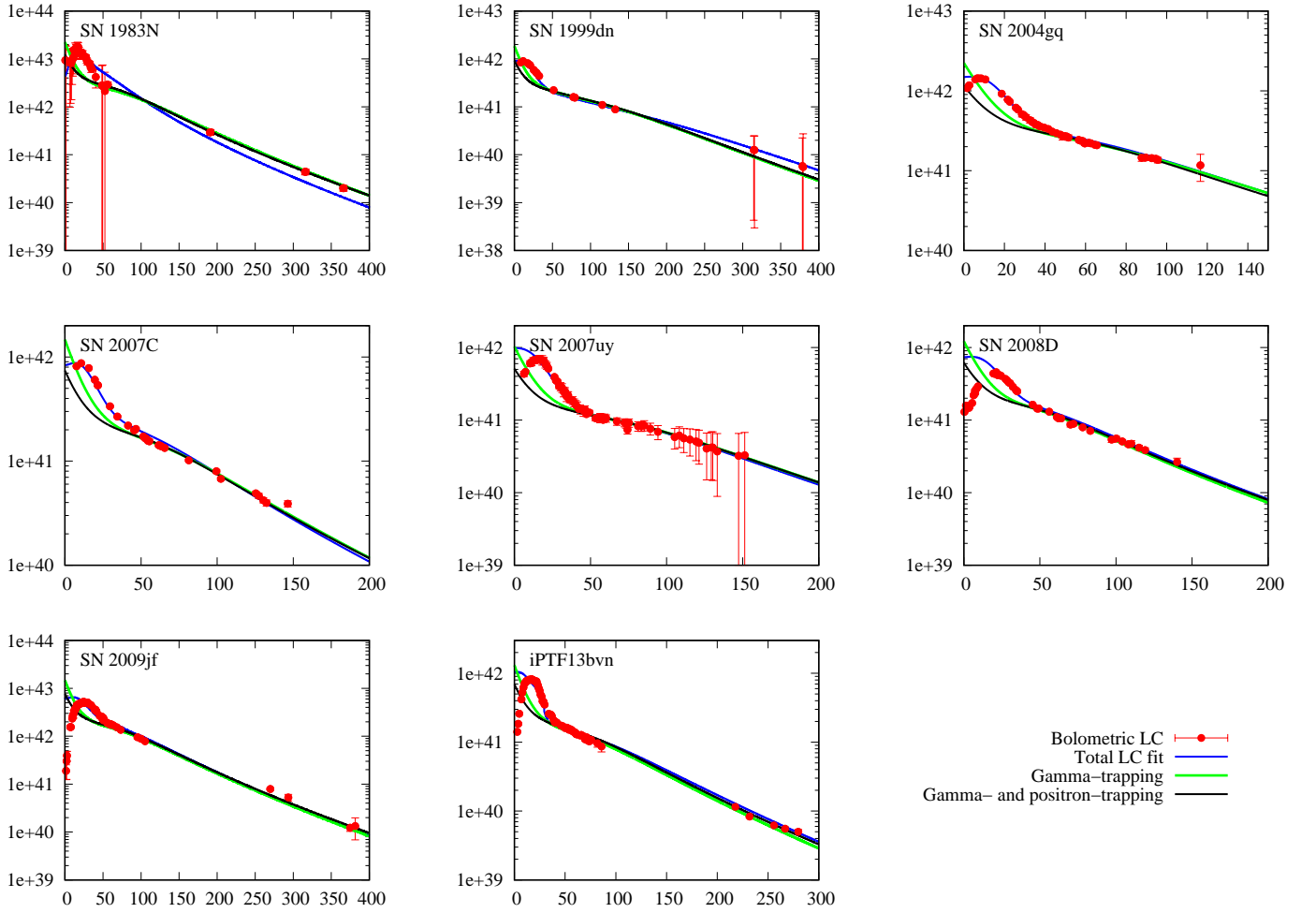


**Figure A2.** Bolometric light curve fits for Type Ib supernovae. The red dots show the observational data with their photometric errors. The blue line represents the best fit for the entire bolometric light curve, while the green and black lines show the late-time LC fits for only gamma-leakage and gamma- and positron-leakage, respectively.

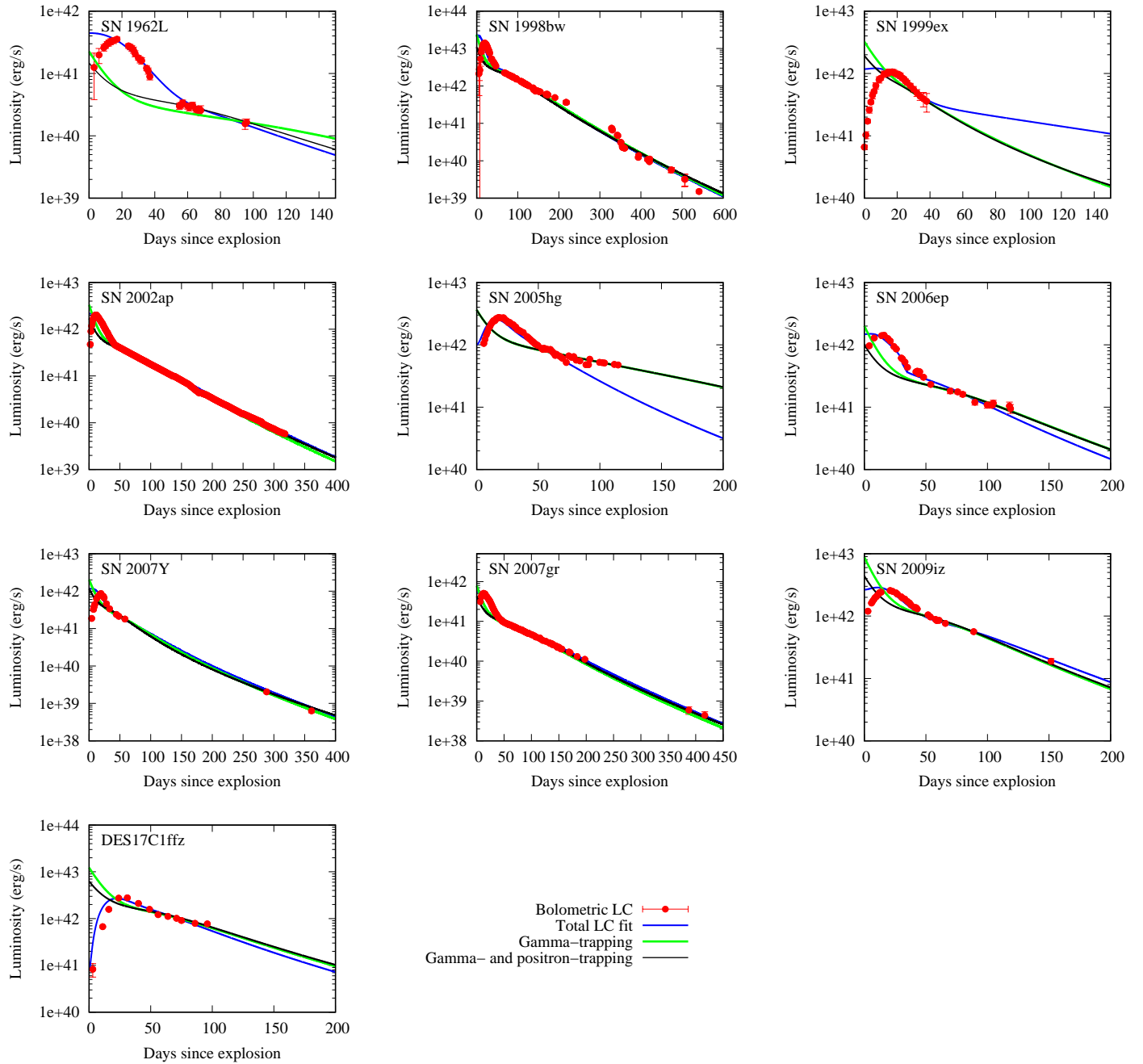


**Figure A3.** Bolometric light curve fits for Type Ibc supernovae. The red dots show the observational data with their photometric errors. The blue line represents the best fit for the entire bolometric light curve, while the green and black lines show the late-time LC fits for only gamma-leakage and gamma- and positron-leakage, respectively.

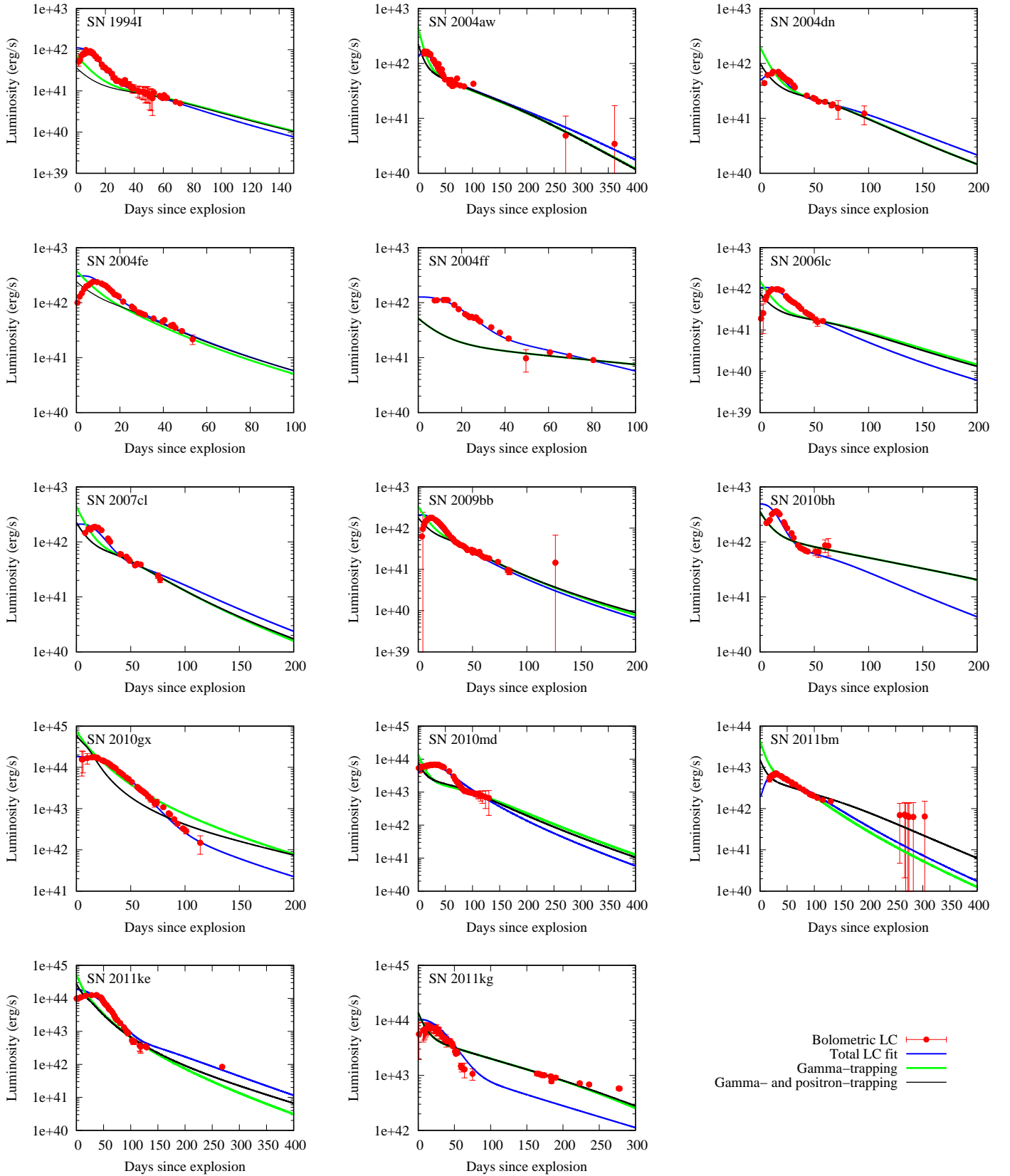


**Figure A4.** Bolometric light curve fits for Type Ic supernovae. The red dots show the observational data with their photometric errors. The blue line represents the best fit for the entire bolometric light curve, while the green and black lines show the late-time LC fits for only gamma-leakage and gamma- and positron-leakage, respectively.

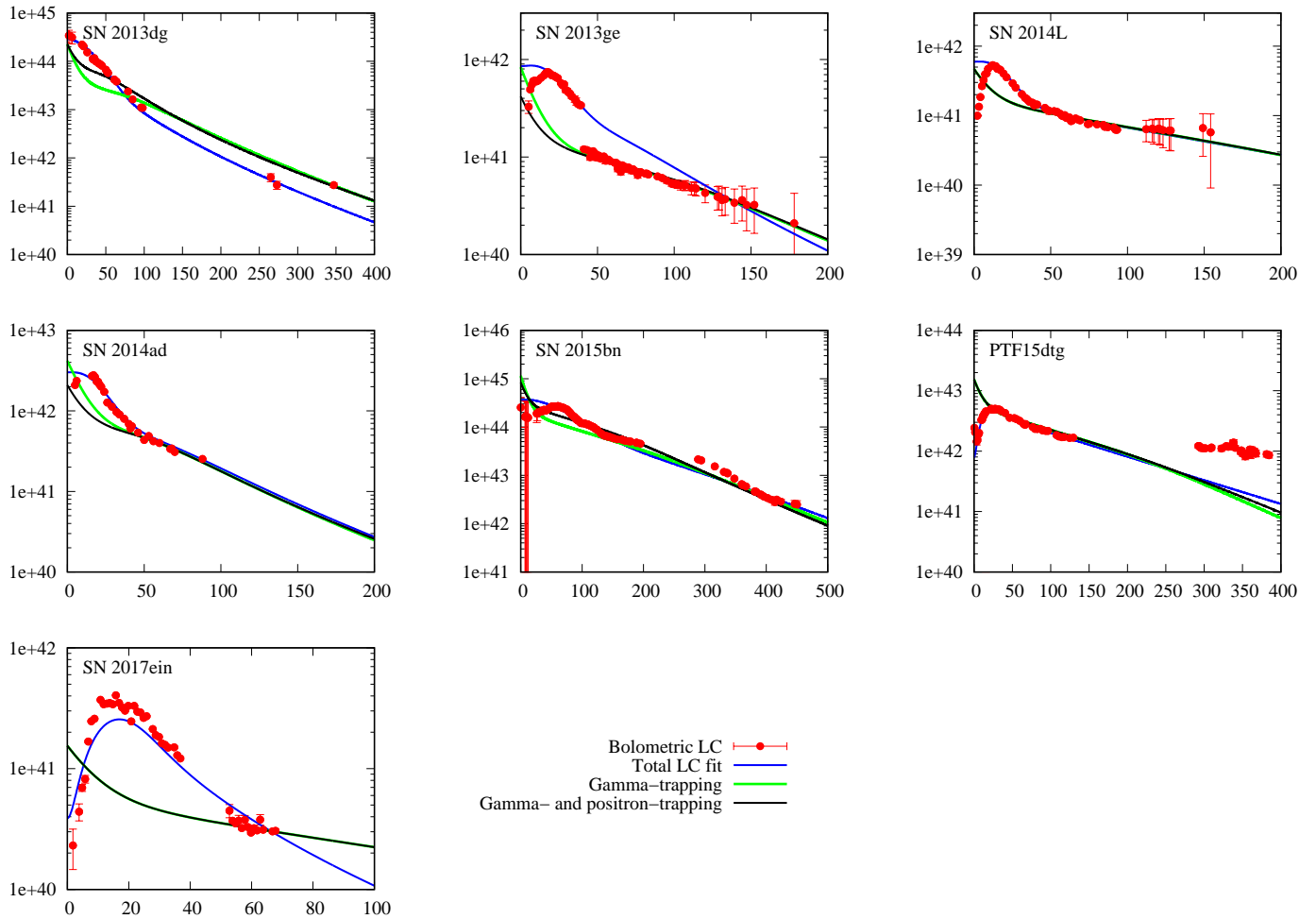


**Figure A5.** Bolometric light curve fits for Type Ic supernovae. The red dots show the observational data with their photometric errors. The blue line represents the best fit for the entire bolometric light curve, while the green and black lines show the late-time LC fits for only gamma-leakage and gamma- and positron-leakage, respectively.

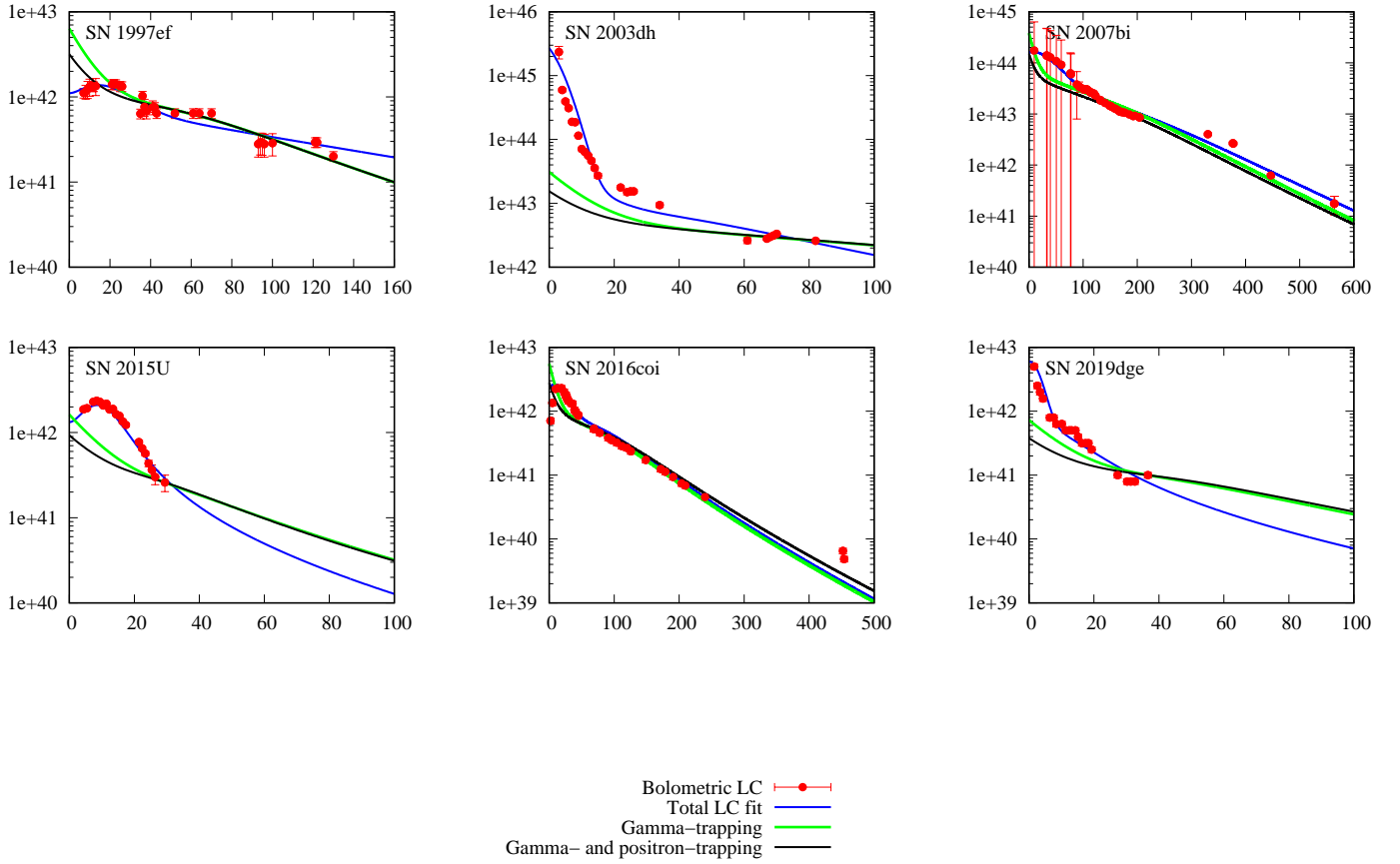


**Figure A6.** Bolometric light curve fits for peculiar SESNe. The red dots show the observational data with their photometric errors. The blue line represents the best fit for the entire bolometric light curve, while the green and black lines show the late-time LC fits for only gamma-leakage and gamma- and positron-leakage, respectively.